



This discussion paper is/has been under review for the journal Atmospheric Measurement Techniques (AMT). Please refer to the corresponding final paper in AMT if available.

Effect of surface BRDF of various land cover types on the geostationary observations of tropospheric NO₂

K. Noguchi¹, A. Richter², V. Rozanov², A. Rozanov², J. P. Burrows², H. Irie³, and K. Kita⁴

¹Nara Women's University, Nara, Japan

²University of Bremen, Bremen, Germany

³Chiba University, Chiba, Japan

⁴Ibaragi University, Ibaragi, Japan

Received: 30 January 2014 – Accepted: 11 March 2014 – Published: 7 April 2014

Correspondence to: K. Noguchi (nogu@ics.nara-wu.ac.jp)

Published by Copernicus Publications on behalf of the European Geosciences Union.

BRDF effect on GEO measurements

K. Noguchi et al.

Title Page

Abstract

Introduction

Conclusions

References

Tables

Figures

◀

▶

◀

▶

Back

Close

Full Screen / Esc

Printer-friendly Version

Interactive Discussion



Abstract

We investigated the effect of surface reflectance anisotropy, Bidirectional Reflectance Distribution Function (BRDF), on satellite retrievals of tropospheric NO₂. We assume the geometry of geostationary measurements over Tokyo, which is one of the worst air-polluted regions in the East Asia. We calculated air mass factors (AMF) and box AMFs (BAMF) for tropospheric NO₂ to evaluate the effect of BRDF by using the radiative transfer model SCIATRAN. To model the BRDF effect, we utilized the Moderate Resolution Imaging Spectroradiometer (MODIS) products (MOD43B1 and MOD43B2), which provide three coefficients to express the RossThick-LiSparseReciprocal model, a semi-empirical and kernel-based model of BRDF. Because BRDF depends on the land cover type, we also utilized the High Resolution Land-Use and Land-Cover Map by the Advanced Land Observing Satellite (ALOS)/Advanced Visible and Near Infrared Radiometer type 2 (AVNIR-2), which classifies the ground pixels over Tokyo into six main types: water, urban, paddy, crop, deciduous forest and evergreen forest. We first develop an empirical model of the three BRDF coefficients for each land cover type over Tokyo, and then apply the model to the calculation of land cover type dependent AMFs and BAMFs. Results show that the variability of AMF among the land types is up to several tens percent, and if we neglect the reflectance anisotropy, the difference from BRDF's AMF reaches 10% or more. The evaluation of the BAMFs calculated shows that not to consider variations in BRDF will cause large errors if the concentration of NO₂ is high close to the surface, although the importance of BRDF for AMFs decreases for large aerosol optical depth (AOD).

1 Introduction

Nitrogen dioxide (NO₂) plays an important role in tropospheric chemistry, and has been measured from space since the late 1990s. The space-borne measurements from the Global Ozone Monitoring Experiment (GOME) (Burrows et al., 1999) and

AMTD

7, 3443–3469, 2014

BRDF effect on GEO measurements

K. Noguchi et al.

Title Page

Abstract

Introduction

Conclusions

References

Tables

Figures

◀

▶

◀

▶

Back

Close

Full Screen / Esc

Printer-friendly Version

Interactive Discussion



**BRDF effect on GEO
measurements**

K. Noguchi et al.

Title Page

Abstract

Introduction

Conclusions

References

Tables

Figures

◀

▶

◀

▶

Back

Close

Full Screen / Esc

Printer-friendly Version

Interactive Discussion



the Scanning Imaging Absorption Spectrometer for Atmospheric Cartography (SCIAMACHY) (Bovensmann et al., 1999) successfully provided the horizontal distributions of several tropospheric minor constituents including NO₂. The GOME and SCIAMACHY instruments have spatial resolutions of 40 km × 320 km and 30 km × 60 km, respectively. Improved spatial resolution of 13 km × 24 km (nadir mode) is achieved by the Ozone Monitoring Instrument (OMI) onboard the Earth Observing System Aura, launched in 2004 (Levelt et al., 2006), followed by GOME-2 with a resolution of 40 km × 80 km (Callies et al., 2000).

In previous studies it was shown that measurements at such a high spatial resolution need more realistic parameters of such as surface pressure, surface albedo and reflectivity to derive accurate tropospheric NO₂ vertical column density (Heckel et al., 2011; Russell et al., 2011). The authors indicated that the error from surface albedo was especially large. One of the difficulties to treat surface albedo is its complex dependence on incident and outgoing direction of light, which is expressed as Bidirectional Reflectance Distribution Function (BRDF). Because the precise observations of BRDF for the entire global surface are difficult, nearly all previous studies assumed Lambertian equivalent reflectivity (LER) surface for the operational retrieval of the NO₂ products. However, Zhou et al. (2010) pointed out the importance of BRDF for the tropospheric NO₂ retrievals, showing that the differences between the tropospheric NO₂ vertical column densities using LER and BRDF are 0–20 %. Lin et al. (2013) accounts for the BRDF effect in the retrievals of the tropospheric NO₂ column density over China using OMI measurements, and the authors showed that no consideration of BRDF in the NO₂ retrievals resulted in the decrease of the tropospheric NO₂ vertical column densities by 7 % on average with the variability of up to 45 % for individual grid pixels compared to the retrievals with the OMI-based LER version 3.

In the present study, we discuss the effect of BRDF on tropospheric NO₂ retrievals in future geostationary measurements from the Geostationary Mission for Meteorology and Air Pollution (GMAP-Asia) in Japan (Akimoto et al., 2008, 2009), where a horizontal resolution of 10 km × 10 km or less is planned. The GMAP-Asia aims at monitoring of air

two coefficients, f_{iso} and f_{vol} , are related with the directional components of the surface reflectance. The details of these coefficients are described in Roujean et al. (1992) and Zhou et al. (2010).

To discuss the BRDF effect, we utilized not only the MODIS derived BRDF but also approximations of BRDF in the calculation of the air mass factor (AMF) and the box air mass factor (BAMF) of the tropospheric NO_2 . Table 1 explains the differences among the approximations used and the BRDF. We calculated AMF and BAMF not only for BRDF but also for Bidirectional Reflectance Factors (BRF), Black-Sky Albedo (BSA) and White-Sky Albedo (WSA) to compare with the results among those definitions.

The three BRDF parameters, f_{iso} , f_{vol} and f_{geo} , are included in the MODIS BRDF product (MOD43B1). We use the product MOD43B2 for a check of the data quality. The spatial resolution of the three BRDF parameters which we utilized in the present study is $1\text{ km} \times 1\text{ km}$. The values of BRF, BSA and WSA are calculated by using the MODIS BRDF parameters and are input into the radiative transfer model (RTM) as LER. As for BRDF, the RTM directly reads the three parameters and then calculates AMF and BAMF considering the BRDF effect.

2.2 Land cover type data

To take into account land cover types in the calculation of BRDF and other albedo types, we utilized the High Resolution Land-Use and Land-Cover Map by ALOS/AVNIR-2 (Fukue et al., 1997). The spatial resolution of the dataset is approximately $50\text{ m} \times 50\text{ m}$. As the grid size of AVNIR-2 is much smaller than that of MODIS, one MODIS grid pixel includes 400 pixels of AVNIR-2 (Fig. 2). Since there are few MODIS pixels which consist of only one land cover type, we define the most frequent land cover type within each MODIS grid pixel as the representative land cover type of the pixel. Figure 3 shows the most dominant land cover type for each MODIS grid pixel over Tokyo. The land-cover types which we focus on in the present study are summarized in Table 2.

BRDF effect on GEO measurements

K. Noguchi et al.

Title Page

Abstract

Introduction

Conclusions

References

Tables

Figures

◀

▶

◀

▶

Back

Close

Full Screen / Esc

Printer-friendly Version

Interactive Discussion



2.3 Atmospheric and geometric scenarios for calculation of AMFs and BAMFs by SCIATRAN

We calculated the AMFs and BAMFs of the tropospheric NO₂ by the RTM SCIA-TRAN (version 3.1.29), which was developed to perform radiative transfer modeling for the purpose of the measurements of the Earth's atmosphere (Rozanov et al., 2005; Rozanov et al., 2014). SCIATRAN can perform radiative transfer calculations properly accounting for the spherical shape of the Earth's atmosphere including refraction. In this study, the discrete-ordinates method, which is one of the options provided by SCIATRAN, was selected to solve the integro-differential radiative transfer equation with pseudo spherical mode.

For the simulations, appropriate atmospheric and geometric scenarios need to be defined. We defined 143 atmospheric layers between the altitudes of 0 km and 100 km with the vertical resolution of 200 m (0–10 km), 500 m (10–12 km) and 1 km (12–100 km). We used a fixed NO₂ vertical profile without seasonal or local time changes (Fig. 4). The scientific requirement team in the GMAP-Asia project provided this NO₂ profile data which is based on the measurements conducted by the TRACE-P aircraft mission (Jacob et al., 2003) and numerical simulations of the WRF/Chem model version 3.0.1 (Grell et al., 2005) with the calculation conditions defined in Takigawa et al. (2007) and also by the CHASER model (Sudo et al., 2002). Pressure and temperature were taken from the US standard atmosphere 1976 (the average of midlatitudes). As for aerosols, we adopted a typical mixing state for urban aerosols described in Hess et al. (1998) with the options prepared by SCIATRAN. Table 1 in Noguchi et al. (2011) summarizes the details of the aerosol conditions assumed in the present study. We also assume a vertical profile of the extinction coefficient with a scale height of 3 km and an aerosol optical depth (AOD) of 0.2 and 1.0 for comparison at a wavelength of 550 nm.

For the definition of the geometric scenario in SCIATRAN, three angles are needed; the SZA, the viewing angle from the satellite and the relative azimuth angle (the angle

BRDF effect on GEO measurements

K. Noguchi et al.

Title Page

Abstract

Introduction

Conclusions

References

Tables

Figures

◀

▶

◀

▶

Back

Close

Full Screen / Esc

Printer-friendly Version

Interactive Discussion



between the sun and the satellite or an observation point at the ground surface). The definitions of those angles in SCIATRAN are depicted in Noguchi et al. (2011). We prepared a diurnal variation of SZAs and relative azimuth angles for summer and winter solstices as shown in Table 3 in Noguchi et al. (2011). The viewing angle is constant for a geostationary satellite; 46.4° at the surface, and 6.3° at the satellite position, which is chosen to be located at the altitude of 36 000 km over 120° E on the equator.

3 Results

3.1 Empirical model of BRDF parameters (f_{iso} , f_{vol} , f_{geo}) specific for land cover types

To obtain an empirical model of the typical BRDF parameters for each land cover type over Tokyo, we computed monthly averages of the BRDF parameters, f_{iso} , f_{vol} and f_{geo} , grouped by MODIS pixels having the same land cover type. As is described in Sect. 2.2, we classify each MODIS pixel to have one specific land cover type, which is the most dominant land cover type in the MODIS pixel. To select typical MODIS pixels which represent each land cover type, we defined a threshold for the percentage of the most frequent AVNIR-2 land cover type in a MODIS pixel. For a sensitivity study, we changed the threshold to be 90 %, 95 % and 100 % except for crop, where we took 60 %, 70 % and 80 % due to the small number of MODIS pixels with high-ratio dominance of crop, and created monthly averages of the three BRDF parameters by land cover type. For example, we averaged all of the BRDF parameters, f_{iso} , f_{vol} and f_{geo} , using only those MODIS pixels which include 95 % or more of the “water” type of AVNIR-2 pixels to obtain the monthly-mean BRDF parameters of the water type for the threshold of 95 %.

The sensitivity study for the threshold shows that the monthly averages of f_{iso} , f_{vol} and f_{geo} for water, deciduous forest and evergreen forest do not vary much if the threshold is increased from 90 % to 100 % (see the Supplement). For the urban and rice paddy types, however, the results for 90 % and 95 % are similar but that for 100 % is different

Title Page

Abstract

Introduction

Conclusions

References

Tables

Figures

◀

▶

◀

▶

Back

Close

Full Screen / Esc

Printer-friendly Version

Interactive Discussion



from the others. This is because the number of the pixels for 100 % is very small for the two land cover types.

Therefore we decided to take a threshold percentage of 95 % land cover type dominance to obtain an empirical model of monthly averages of the BRDF parameters, f_{iso} , f_{vol} and f_{geo} , except for crop, for which we took a threshold of 70 %. Figure 5 shows the results. We can see that the urban type, which is a major land cover type in the polluted region, has small seasonal dependence. This is consistent with the fact that urban surface features (e.g., buildings and roads) are basically permanent, although plants beside roads and in parks possibly bring about some seasonality.

Deciduous and evergreen forests have a contrastive seasonality; the BRDF parameters of the deciduous forest type largely depend on season, but the evergreen forest type has a relatively small seasonality. The difference is caused by winter leaf drop in deciduous forests. As for the variability of the BRDF parameters (i.e., the magnitude of error bars), the land types covered with plants tend to have large magnitudes than those of urban regions. If we strictly remove the pixels covered by plants from the urban region's pixels, it may decrease the uncertainties related to BRDF's seasonality.

Here we focus on the seasonal change of rice paddy; rice paddy is distributed broadly in plain regions in Japan and also around Tokyo (see Fig. 3). The f_{geo} and f_{vol} of the rice paddy type changes abruptly to close to zero in summer. This is caused by the nature of the water type, which has almost zero values throughout the year for both f_{vol} and f_{geo} , which represent directional components of BRDF. This means that the water type has no directional dependence of scattering (except for sun glint reflection). The seasonal change of rice paddy is caused by water cover in summer, while in other seasons no water exists in a rice paddy. We should note such an abrupt change of the BRDF characteristics during that season in scenes covered by rice paddies which often surround urban regions in Japan.

BRDF effect on GEO measurements

K. Noguchi et al.

Title Page

Abstract

Introduction

Conclusions

References

Tables

Figures

◀

▶

◀

▶

Back

Close

Full Screen / Esc

Printer-friendly Version

Interactive Discussion



3.2 Tropospheric NO₂ AMFs including the BRDF effect for each land cover type

Tropospheric NO₂ AMFs for the BRDF surface are calculated for each land type (Fig. 6). The results show that the AMFs largely depend on land cover type, and the order of the AMF's magnitude between the different land cover types depends on season; in summer the AMF over urban surfaces is largest, while in winter the rice paddy areas have the largest AMF. The AMF of evergreen forest is smallest both in summer and winter. The difference between the largest and smallest AMF is up to several tens percent or even a factor of two. The variability among the land cover types is larger in summer than in winter and stronger at noon than in the morning or evening, which suggests that the dependence of BRDF on land cover types becomes significant when the SZA is small.

Figure 7 shows the relative difference of the AMFs for calculations using approximated surface types, A_{BRF} , A_{BSA} and A_{WSA} , from the AMF for full BRDF treatment, A_{BRDF} . The difference depends in a complex way on season and local time differences from A_{BRDF} being as large as 10% or more. With the exception of water and paddy surfaces, all land types show a similar behavior, indicating that the differences are mainly their total reflectivity and not the angular distribution. For the water covered surfaces, the differences from A_{BRDF} are generally small. In summer, the difference is zero since f_{vol} and f_{geo} of water are zero. The AMF of rice paddies in summer also has a small difference from A_{BRDF} , which is similar with water, since it is filled by water during this season as discussed in Sect. 3.1. This means that A_{BRDF} of rice paddies largely depends on season.

3.3 Tropospheric NO₂ BAMFs including the BRDF effect for each land cover type

Figure 8 shows the vertical profile of BAMF for each land cover type calculated with full treatment of BRDF. The figure indicates that the BAMF differences among land cover

Title Page

Abstract

Introduction

Conclusions

References

Tables

Figures

◀

▶

◀

▶

Back

Close

Full Screen / Esc

Printer-friendly Version

Interactive Discussion



**BRDF effect on GEO
measurements**

K. Noguchi et al.

Title Page

Abstract

Introduction

Conclusions

References

Tables

Figures

◀

▶

◀

▶

Back

Close

Full Screen / Esc

Printer-friendly Version

Interactive Discussion



types become larger in the lower layers. This means that the AMF dependence on the land cover types shown in Sect. 3.2 is mainly caused by the BAMF variability in the lower altitudes. As a result it follows that wherever a high concentration of NO_2 exists in the lower layers, the AMF's difference among land cover types will become large.

Figure 9 shows the relative differences of the BAMFs for B_{BRF} from the BAMF for full BRDF treatment, B_{BRDF} . The results for B_{BSA} and B_{WSA} are shown in the Supplement. The difference from B_{BRDF} becomes larger in the lower altitudes, and the differences can be larger than 10%. The results for B_{BSA} and B_{WSA} are also similar with the results for B_{BRDF} . This suggests that using BRF, BSA or WSA instead of BRDF as an approximation of the surface albedo causes an altitude-dependent error, and if a high concentration of NO_2 exists in the lower layers, the difference will become large.

3.4 Effect of aerosols

Figure 10 shows the relative difference of the AMFs for approximated BRDF surface types, A_{BRF} , A_{BSA} and A_{WSA} , from the AMF for BRDF, A_{BRDF} for AOD of 1.0. Compared with Fig. 7, where AOD of 0.2 is assumed, smaller variability of AMF can be seen among land cover types. This can be attributed to the fact that larger scattering of aerosols weakens importance of the surface term on the radiation field and thus decreases the dependence on the BRDF of different land cover types. Figure 10 also indicates that the AMF computed using the WSA has the smallest difference from that based on the full BRDF. This suggests that not considering the angular dependence at all (i.e., WSA) is better than an incomplete implementation (i.e., BRF and BSA) of angle dependence. In summary, the importance of BRDF on the AMFs decreases for increasing AOD.

4 Concluding remarks

Assuming a geostationary satellite monitoring, we investigated the effect of surface reflectance anisotropy, BRDF on the tropospheric NO₂ measurements by calculating AMF and BAMF for different BRDF types. Besides BRDF, which fully considers surface reflectance anisotropy, we took three albedo types (BRF, BSA, WSA), which have a different level of the consideration of surface reflectance anisotropy as an approximation. In our calculations, we also considered six land cover types: water, urban, paddy, crop, deciduous forest and evergreen forest and their respective seasonal BRDFs.

Using MODIS BRDF results with AVNIR-2 land cover map data, we first developed an empirical model of BRDF parameters (f_{iso} , f_{vol} , f_{geo}) specific for land cover types representative for the Tokyo area. Using the empirical model, we calculated AMFs and BAMFs for tropospheric NO₂ by SCIATRAN. Results show that the AMF for tropospheric NO₂ largely depends on land cover types; the variability among the land types is up to several tens percent. If we neglect the reflectance anisotropy (i.e., use BRF, BSA or WSA), the difference from AMF_{BRDF} reaches 10 % or more. The difference depends in a complicated way on season and local time. Incomplete implementation of surface reflectance anisotropy (i.e., BRF and BSA) can bring about even worse results than not considering the anisotropy of reflectance at all (i.e., WSA). In the lower altitudes, the BAMF difference among land cover types becomes larger. The difference of BAMFs computed using the BRF, BSA and WSA from those derived using full BRDF treatment is also larger in the lower layers. If a high concentration of the tropospheric NO₂ exists in the lower altitudes, failure to consider variations or BRDF will cause larger errors of the AMF. At larger AOD (1.0), the differences in AMFs for the various surface types become smaller indicating that the importance of BRDF decreases for large AOD.

In the present study, we rely on the MODIS-derived BRDF coefficients to be correct for all geometries and surfaces that we investigate. However, the assumption could be a source of uncertainty in the calculation of AMFs and BAMFs. More comparison and validation of satellite-based BRDF measurements (e.g., Susaki et al. (2004) for a rice

BRDF effect on GEO measurements

K. Noguchi et al.

Title Page

Abstract

Introduction

Conclusions

References

Tables

Figures

◀

▶

◀

▶

Back

Close

Full Screen / Esc

Printer-friendly Version

Interactive Discussion



paddy) will be needed by independent satellite measurements and ground measurements.

Supplementary material related to this article is available online at

<http://www.atmos-meas-tech-discuss.net/7/3443/2014/>

[amtd-7-3443-2014-supplement.pdf](#)

Acknowledgements. We would like to thank Yasuko Kasai and other members of the APOLLO project and the Japan Society of Atmospheric Chemistry. We would also like to thank Kanako Muramatsu and Noriko Soyama for their useful comments on surface albedo. For the calculation of the SZA and other angles, we utilized the website of the National Astronomical Observatory of Japan (<http://www.nao.ac.jp/koyomi/koyomix/koyomix.html>). The MODIS products were available at the NASA's website, <https://wist.echo.nasa.gov/> (now changed to https://lpdaac.usgs.gov/data_access/data_pool) The High Resolution Land-Use and Land-Cover Map is available at the JAXA's website, http://www.eorc.jaxa.jp/ALOS/lulc/lulc_jindex.htm. This work was supported by JSPS KAKENHI Grant Numbers 24710008 (K. Noguchi) and 22310004 (K. Kita). This work was carried out partly by the joint research program of CEReS, Chiba University (2013). This research was partly supported by the Coordination Funds for Promoting Space Utilization by the Education, Culture, Sports, Science and Technology (MEXT), JAPAN.

References

- Akimoto, H., Kasai, Y., and Kita, K. (Eds.): Planning a Geostationary Atmospheric Observation Satellite, National Institute of Information and Communications Technology, 2008. 3445
- Akimoto, H., Kasai, Y., Kita, K., Irie, H., Sagi, K., and Hayashida, S.: Geostationary Atmospheric Observation Satellite Plan in Japan (invited), AGU Fall Meeting Abstracts, A51M-01, 2009. 3445
- Bovensmann, H., Burrows, J. P., Buchwitz, M., Frerick, J., Noël, S., Rozanov, V. V., Chance, K. V., and Goede, A. P. H.: SCIAMACHY: mission objectives and measurement modes, *J. Atmos. Sci.*, 56, 127–150, doi:10.1175/1520-0469(1999)056<0127:SMOAMM>2.0.CO;2, 1999. 3445

BRDF effect on GEO measurements

K. Noguchi et al.

Title Page

Abstract

Introduction

Conclusions

References

Tables

Figures

◀

▶

◀

▶

Back

Close

Full Screen / Esc

Printer-friendly Version

Interactive Discussion



**BRDF effect on GEO
measurements**

K. Noguchi et al.

Title Page

Abstract

Introduction

Conclusions

References

Tables

Figures

◀

▶

◀

▶

Back

Close

Full Screen / Esc

Printer-friendly Version

Interactive Discussion



Burrows, J. P., Weber, M., Buchwitz, M., Rozanov, V., Ladstätter-Weißenmayer, A., Richter, A., Debeek, R., Hoogen, R., Bramstedt, K., Eichmann, K.-U., Eisinger, M., and Perner, D.: The Global Ozone Monitoring Experiment (GOME): mission concept and first scientific results, *J. Atmos. Sci.*, 56, 151–175, doi:10.1175/1520-0469(1999)056<0151:TGOMEG>2.0.CO;2, 1999. 3444

Callies, J., Corpaccioli, E., Eisinger, M., Hahne, A., and Lefebvre, A.: GOME-2 Metop's second-generation sensor for operational ozone monitoring, *ESA Bull.*, 102, 28–36, 2000. 3445

Fukue, K., Igarashi, T., Osawa, Y., Shimoda, H., Matsuoka, R., and Kawata, Y.: Advanced Visible and Near-Infrared Radiometer type 2 (AVNIR-2), in: Society of Photo-Optical Instrumentation Engineers (SPIE) Conference Series, edited by: Fujisada, H., Calamai, G., and Sweeting, M. N., Vol. 2957 of Society of Photo-Optical Instrumentation Engineers (SPIE) Conference Series, 208–215, 1997. 3447

Grell, G. A., Peckham, S. E., Schmitz, R., McKeen, S. A., Frost, G., Skamarock, W. C., and Eder, B.: Fully coupled “online” chemistry within the WRF model, *Atmos. Environ.*, 39, 6957–6975, doi:10.1016/j.atmosenv.2005.04.027, 2005. 3448

Heckel, A., Kim, S.-W., Frost, G. J., Richter, A., Trainer, M., and Burrows, J. P.: Influence of low spatial resolution a priori data on tropospheric NO₂ satellite retrievals, *Atmos. Meas. Tech.*, 4, 1805–1820, doi:10.5194/amt-4-1805-2011, 2011. 3445

Hess, M., Koepke, P., and Schult, I.: Optical Properties of Aerosols and Clouds: the software package OPAC, *Bull. Am. Meteorol. Soc.*, 79, 831–844, doi:10.1175/1520-0477(1998)079<0831:OPOAAC>2.0.CO;2, 1998. 3448

Jacob, D. J., Crawford, J. H., Kleb, M. M., Connors, V. S., Bendura, R. J., Raper, J. L., Sachse, G. W., Gille, J. C., Emmons, L., and Heald, C. L.: Transport and Chemical Evolution over the Pacific (TRACE-P) aircraft mission: design, execution, and first results, *J. Geophys. Res.-Atmos.*, 108, 9000, doi:10.1029/2002JD003276, 2003. 3448

Justice, C., Vermote, E., Townshend, J., Defries, R., Roy, D., Hall, D., Salomonson, V., Privette, J., Riggs, G., Strahler, A., Lucht, W., Myneni, R., Knyazikhin, Y., Running, S., Nemani, R., Wan, Z., Huete, A., van Leeuwen, W., Wolfe, R., Giglio, L., Muller, J., Lewis, P., and Barnsley, M.: The Moderate Resolution Imaging Spectroradiometer (MODIS): land remote sensing for global change research, *IEEE T. Geosci. Remote*, 36, 1228–1249, doi:10.1109/36.701075, 1998. 3446

**BRDF effect on GEO
measurements**

K. Noguchi et al.

Title Page

Abstract

Introduction

Conclusions

References

Tables

Figures

◀

▶

◀

▶

Back

Close

Full Screen / Esc

Printer-friendly Version

Interactive Discussion



- Levelt, P. F., van den Oord, G. H. J., Dobber, M. R., Malkki, A., Visser, H., de Vries, J., Stammes, P., Lundell, J. O. V., and Saari, H.: The ozone monitoring instrument, *IEEE T. Geosci. Remote*, 44, 1093–1101, doi:10.1109/TGRS.2006.872333, 2006. 3445
- Lin, J.-T., Martin, R. V., Boersma, K. F., Sneep, M., Stammes, P., Spurr, R., Wang, P., Van Roozendaal, M., Clémer, K., and Irie, H.: Retrieving tropospheric nitrogen dioxide over China from the Ozone Monitoring Instrument: effects of aerosols, surface reflectance anisotropy and vertical profile of nitrogen dioxide, *Atmos. Chem. Phys. Discuss.*, 13, 21203–21257, doi:10.5194/acpd-13-21203-2013, 2013. 3445
- Lucht, W., Schaaf, C., and Strahler, A.: An algorithm for the retrieval of albedo from space using semiempirical BRDF models, *IEEE T. Geosci. Remote*, 38, 977–998, doi:10.1109/36.841980, 2000. 3446
- Noguchi, K., Richter, A., Bovensmann, H., Hilboll, A., Burrows, J. P., Irie, H., Hayashida, S., and Morino, Y.: A feasibility study for the detection of the diurnal variation of tropospheric NO₂ over Tokyo from a geostationary orbit, *Adv. Space. Res.*, 48, 1551–1564, doi:10.1016/j.asr.2011.06.029, 2011. 3448, 3449
- Roujean, J.-L., Leroy, M., and Deschamps, P.-Y.: A bidirectional reflectance model of the Earth's surface for the correction of remote sensing data, *J. Geophys. Res.-Atmos.*, 97, 20455–20468, doi:10.1029/92JD01411, 1992. 3446, 3447
- Rozanov, A., Rozanov, V., Buchwitz, M., Kokhanovsky, A., and Burrows, J. P.: SCIATRAN 2.0 – a new radiative transfer model for geophysical applications in the 175–2400 nm spectral region, *Adv. Space Res.*, 36, 1015–1019, doi:10.1016/j.asr.2005.03.012, 2005. 3448
- Rozanov, V., Rozanov, A., Kokhanovsky, A., and Burrows, J.: Radiative transfer through terrestrial atmosphere and ocean: software package SCIATRAN, *J. Quant. Spectrosc. Ra.*, 133, 13–71, doi:10.1016/j.jqsrt.2013.07.004, 2014. 3448
- Russell, A. R., Perring, A. E., Valin, L. C., Bucsela, E. J., Browne, E. C., Wooldridge, P. J., and Cohen, R. C.: A high spatial resolution retrieval of NO₂ column densities from OMI: method and evaluation, *Atmos. Chem. Phys.*, 11, 8543–8554, doi:10.5194/acp-11-8543-2011, 2011. 3445
- Sudo, K., Takahashi, M., Kurokawa, J., and Akimoto, H.: CHASER: a global chemical model of the troposphere 1. Model description, *J. Geophys. Res.-Atmos.*, 107, 4339, doi:10.1029/2001JD001113, 2002. 3448

- Susaki, J., Hara, K., Park, J., Yasuda, Y., Kajiwara, K., and Honda, Y.: Validation of temporal BRDFs of paddy fields estimated from MODIS reflectance data, IEEE T. Geosci. Remote, 42, 1262–1270, doi:10.1109/TGRS.2004.826798, 2004. 3453
- 5 Takigawa, M., Niwano, M., Akimoto, H., and Takahashi, M.: Development of a one-way nested global-regional air quality forecasting model, SOLA, 3, 81–84, doi:10.2151/sola.2007-021, 2007. 3448
- Zhou, Y., Brunner, D., Spurr, R. J. D., Boersma, K. F., Sneep, M., Popp, C., and Buchmann, B.: Accounting for surface reflectance anisotropy in satellite retrievals of tropospheric NO₂, Atmos. Meas. Tech., 3, 1185–1203, doi:10.5194/amt-3-1185-2010, 2010. 3445, 3447

BRDF effect on GEO measurements

K. Noguchi et al.

Title Page

Abstract

Introduction

Conclusions

References

Tables

Figures

◀

▶

◀

▶

Back

Close

Full Screen / Esc

Printer-friendly Version

Interactive Discussion



BRDF effect on GEO measurements

K. Noguchi et al.

Title Page

Abstract

Introduction

Conclusions

References

Tables

Figures

◀

▶

◀

▶

Back

Close

Full Screen / Esc

Printer-friendly Version

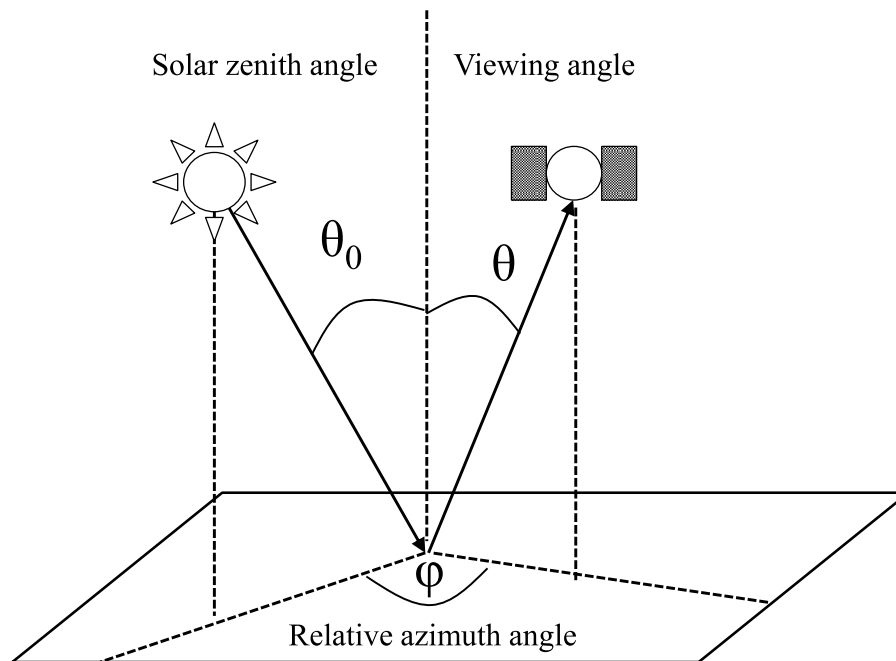
Interactive Discussion

**Table 1.** Definition of surface albedo types used in the present study.

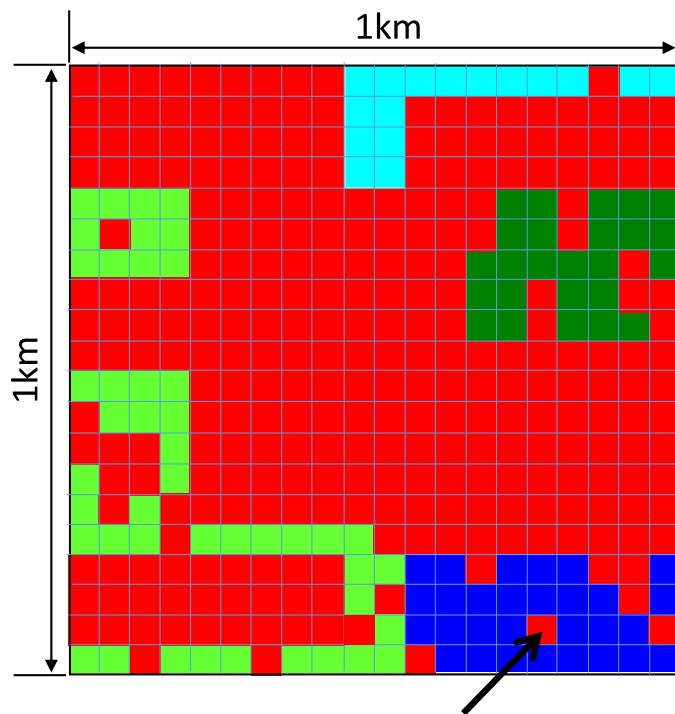
albedo type	definition
BRDF	Full consideration of surface reflectance anisotropy in radiative transfer model (RTM)
BRF (Bidirectional Reflectance Factors)	Angle dependence (θ_0, θ, ϕ) is fully considered, but treated as Lambertian equivalent reflectivity (LER) in RTM
BSA (Black-Sky Albedo)	Only SZA dependence is considered, and treated as LER in RTM
WSA (White-Sky Albedo)	No consideration of angle dependence, and treated as LER in RTM

**BRDF effect on GEO
measurements**

K. Noguchi et al.

**Fig. 1.** Definition of geometry angles of BRDF.[Title Page](#)[Abstract](#)[Introduction](#)[Conclusions](#)[References](#)[Tables](#)[Figures](#)[◀](#)[▶](#)[◀](#)[▶](#)[Back](#)[Close](#)[Full Screen / Esc](#)[Printer-friendly Version](#)[Interactive Discussion](#)

MODIS pixel (1km x 1km)



AVNIR-2 pixel
(50m x 50m)

Fig. 2. Schematic of the MODIS and AVNIR-2 pixel sizes. For example, the dominance of the land cover type shown in red for the MODIS pixel is calculated by dividing the number of the pixels in red (= 285) by the number of all the pixels (= 400).

BRDF effect on GEO measurements

K. Noguchi et al.

Title Page

Abstract Introduction

Conclusions References

Tables Figures

◀ ▶

◀ ▶

Back Close

Full Screen / Esc

Printer-friendly Version

Interactive Discussion



**BRDF effect on GEO
measurements**

K. Noguchi et al.

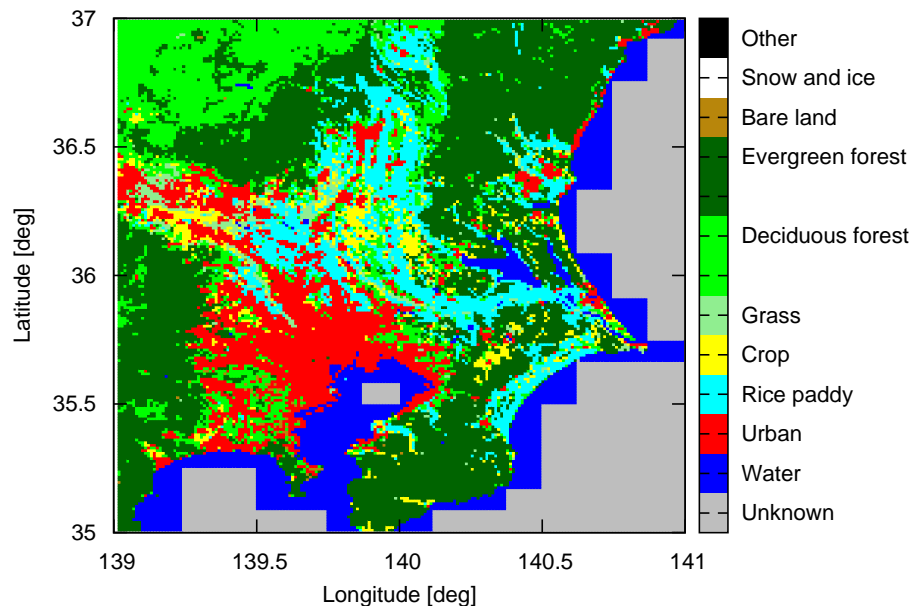


Fig. 3. Land cover type map over the Kanto plain derived by AVNIR-2. The grid size is changed to a 1 km square, which is the MODIS pixel size, from the AVNIR-2 original size of a 50 m square.

[Title Page](#)[Abstract](#)[Introduction](#)[Conclusions](#)[References](#)[Tables](#)[Figures](#)[◀](#)[▶](#)[◀](#)[▶](#)[Back](#)[Close](#)[Full Screen / Esc](#)[Printer-friendly Version](#)[Interactive Discussion](#)

BRDF effect on GEO
measurements

K. Noguchi et al.

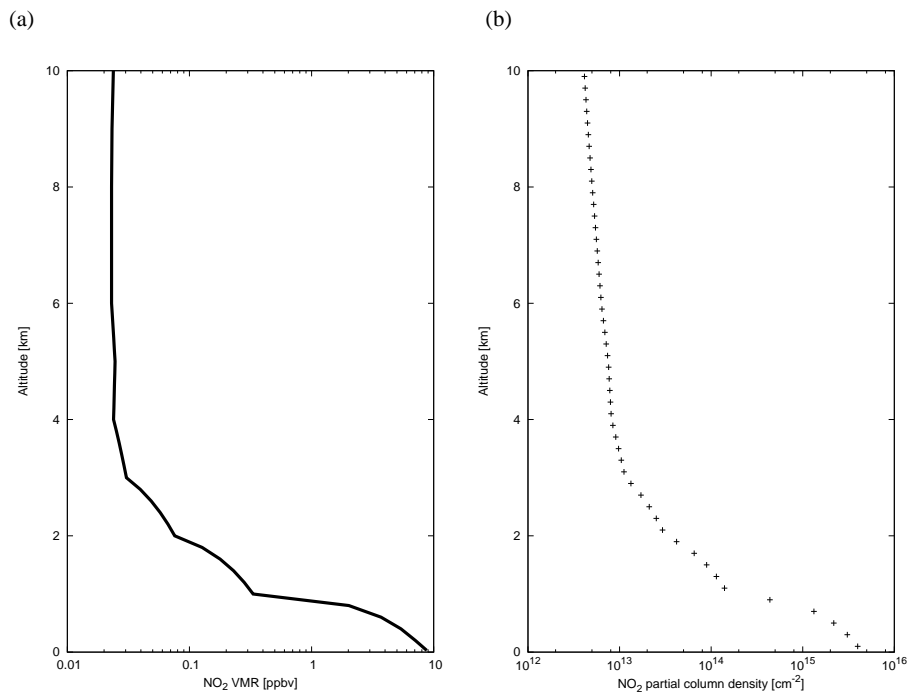


Fig. 4. Vertical profiles of **(a)** NO₂ volume mixing ratio (VMR) and **(b)** NO₂ partial column density of each layer. Tropospheric (0–10 km) total column density is 1.1×10^{16} [cm⁻²].

[Title Page](#)[Abstract](#)[Introduction](#)[Conclusions](#)[References](#)[Tables](#)[Figures](#)[◀](#)[▶](#)[◀](#)[▶](#)[Back](#)[Close](#)[Full Screen / Esc](#)[Printer-friendly Version](#)[Interactive Discussion](#)

BRDF effect on GEO measurements

K. Noguchi et al.

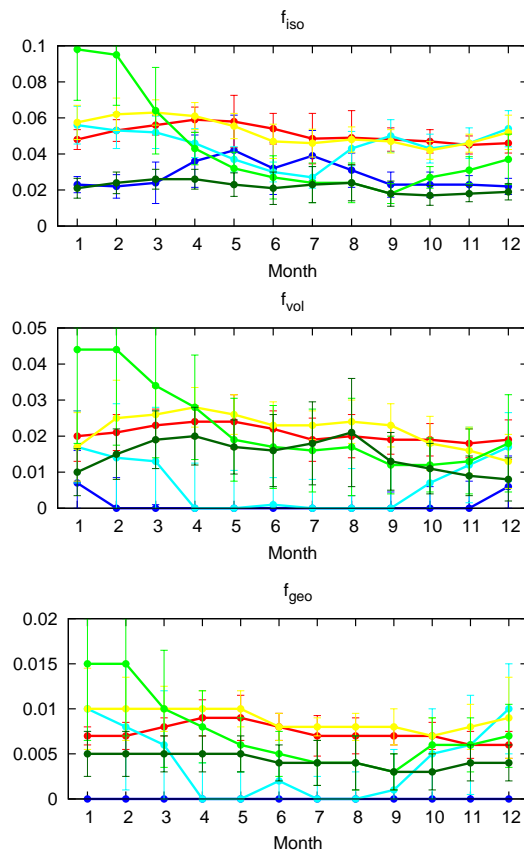


Fig. 5. Monthly averages of the MODIS BRDF parameters, f_{iso} , f_{vol} and f_{geo} for water (blue), urban (red), rice paddy (light blue), crop (yellow), deciduous forest (light green) and evergreen forest (green). The land cover type is derived by AVNIR-2.

BRDF effect on GEO measurements

K. Noguchi et al.

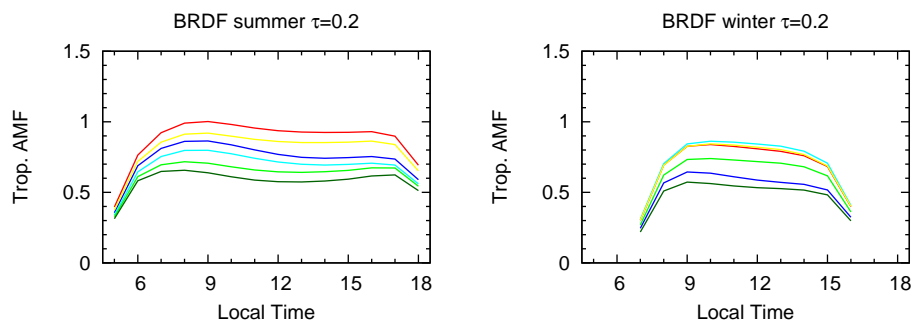


Fig. 6. Tropospheric NO_2 AMF in summer (left) and winter (right) using BRDF surface. The colors indicate land cover types: water (blue), urban (red), rice paddy (light blue), crop (yellow), deciduous forest (light green) and evergreen forest (green). For all calculations an aerosol optical depth (AOD) of 0.2 is assumed.

[Title Page](#)[Abstract](#)[Introduction](#)[Conclusions](#)[References](#)[Tables](#)[Figures](#)[◀](#)[▶](#)[◀](#)[▶](#)[Back](#)[Close](#)[Full Screen / Esc](#)[Printer-friendly Version](#)[Interactive Discussion](#)

BRDF effect on GEO measurements

K. Noguchi et al.

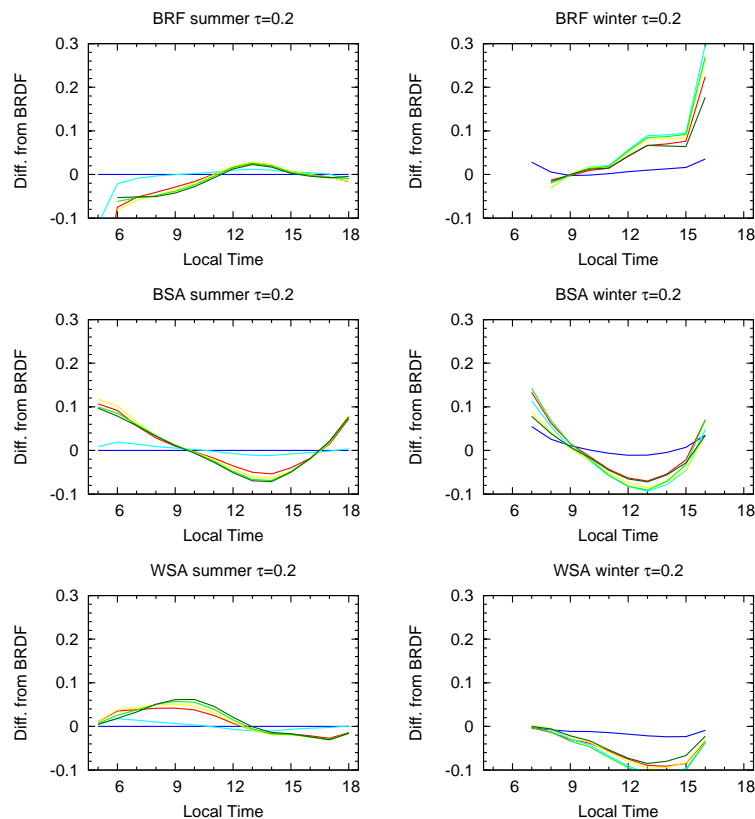


Fig. 7. Relative difference of tropospheric NO_2 AMFs from the value obtained with full BRDF treatment in summer (left) and winter (right) when using BRF (top), BSA (middle) and WSA (bottom) surface. The colors indicate land cover types: water (blue), urban (red), rice paddy (light blue), crop (yellow), deciduous forest (light green) and evergreen forest (green). An aerosol optical depth (AOD) of 0.2 is assumed.

BRDF effect on GEO
measurements

K. Noguchi et al.

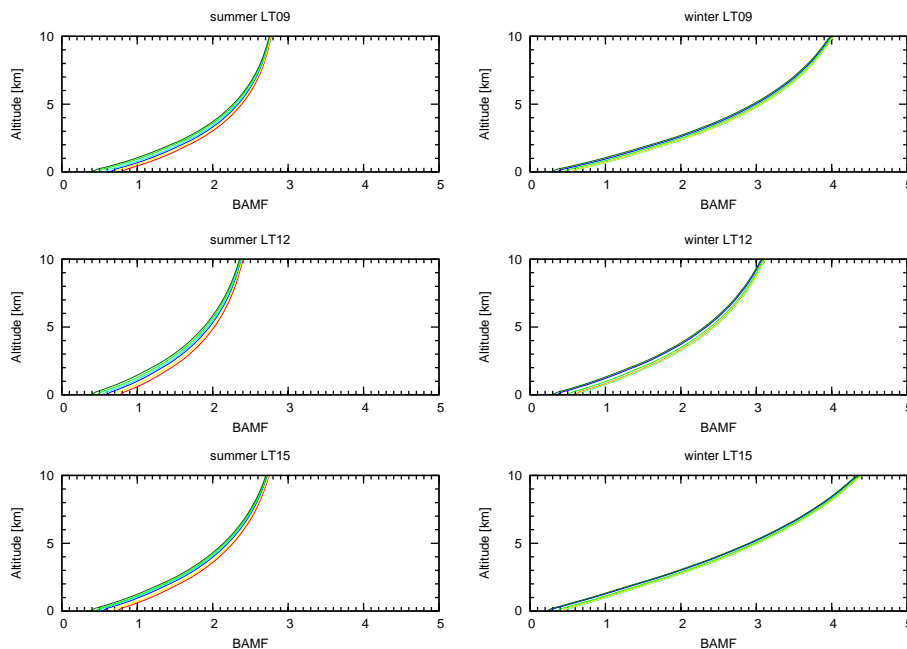


Fig. 8. Tropospheric NO_2 BAMF at local time (LT) 09, LT12 and LT15 in summer (left) and winter (right). The colors indicate land cover types: water (blue), urban (red), rice paddy (light blue), crop (yellow), deciduous forest (light green) and evergreen forest (green). An aerosol optical depth (AOD) of 0.2 is assumed.

[Title Page](#)[Abstract](#)[Introduction](#)[Conclusions](#)[References](#)[Tables](#)[Figures](#)[◀](#)[▶](#)[◀](#)[▶](#)[Back](#)[Close](#)[Full Screen / Esc](#)[Printer-friendly Version](#)[Interactive Discussion](#)

BRDF effect on GEO measurements

K. Noguchi et al.

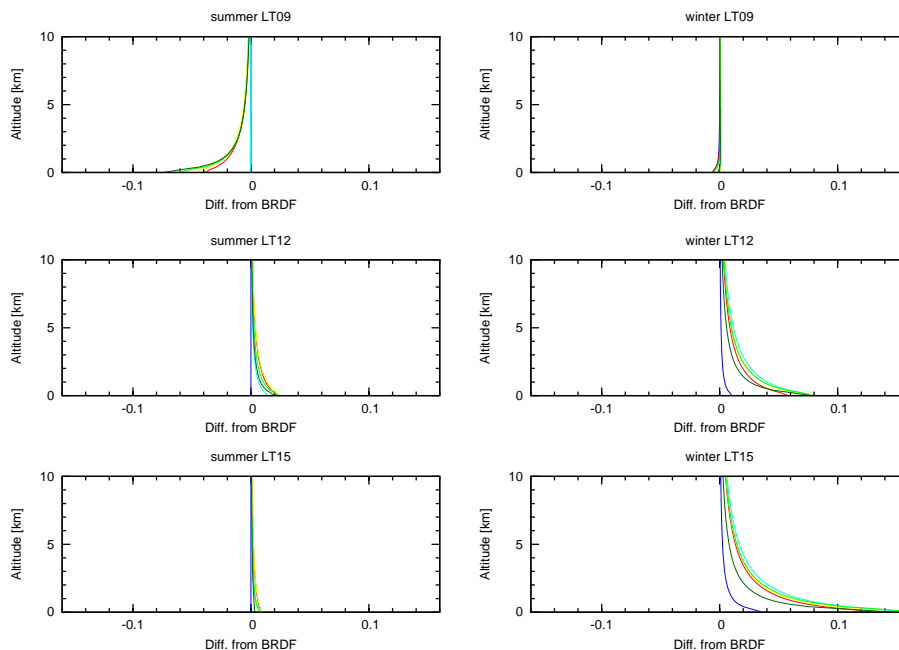


Fig. 9. Relative difference of tropospheric NO_2 BAMF for various land cover types from the tropospheric NO_2 BAMF obtained using full BRDF treatment compared to results using BR surface. Panels at local time (LT) 09, LT12 and LT15 for summer (left) and winter (right) are shown. The colors indicate land cover types: water (blue), urban (red), rice paddy (light blue), crop (yellow), deciduous forest (light green) and evergreen forest (green). An aerosol optical depth (AOD) of 0.2 is assumed.

BRDF effect on GEO measurements

K. Noguchi et al.

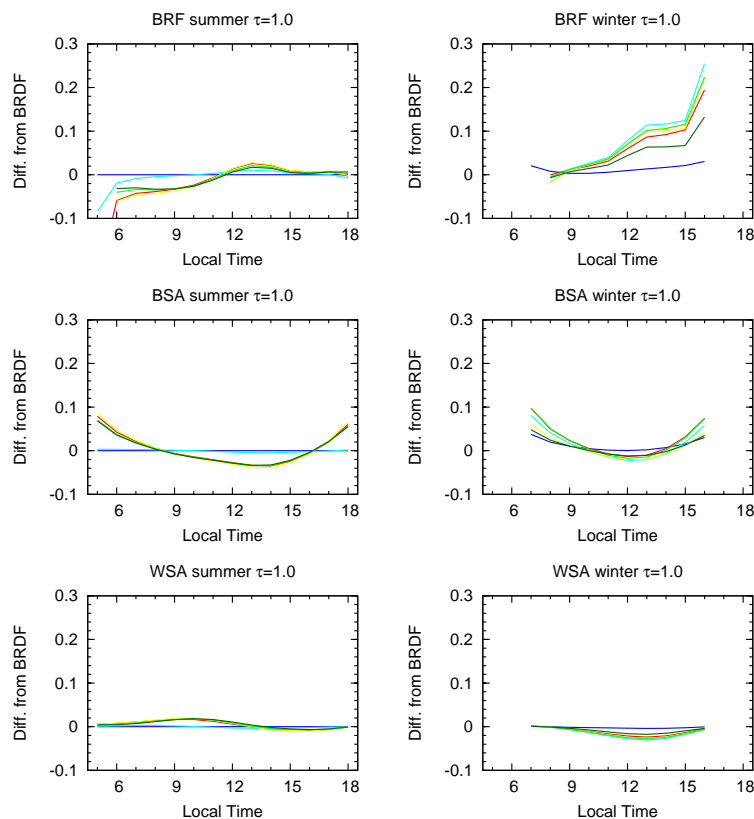


Fig. 10. Relative difference of tropospheric NO_2 AMFs from the value obtained with full BRDF treatment in summer (left) and winter (right) when using BRF (top), BSA (middle) and WSA (bottom) surface. The colors indicate land cover types: water (blue), urban (red), rice paddy (light blue), crop (yellow), deciduous forest (light green) and evergreen forest (green). An aerosol optical depth (AOD) of 1.0 is assumed.